


Crystal structure of toceranib, C₂₂H₂₅FN₄O₂James A. Kaduk ^{1,2,a)} Stacy Gates-Rector ³ and Thomas N. Blanton ³¹Illinois Institute of Technology, 3101 S. Dearborn St., Chicago, IL 60616, USA²North Central College, 131 S. Loomis St., Naperville, IL 60540, USA³ICDD, 12 Campus Blvd., Newtown Square, PA 19073-3273, USA

(Received 11 August 2022; accepted 23 September 2022)

The crystal structure of toceranib has been solved and refined using synchrotron X-ray powder diffraction data, and optimized using density functional theory techniques. Toceranib crystallizes in space group $P2_1/c$ (#14) with $a = 10.6899(6)$, $b = 24.5134(4)$, $c = 7.8747(4)$ Å, $\beta = 107.7737(13)^\circ$, $V = 1965.04(3)$ Å³, and $Z = 4$. The crystal structure consists of stacks of approximately planar molecules, with N–H...O hydrogen bonds between the layers. The commercial reagent sample was a mixture of two or more phases with toceranib being the dominant phase. The difference between the Rietveld-refined and DFT-optimized structures is larger than usual. The powder pattern has been submitted to ICDD for inclusion in the Powder Diffraction File™ (PDF®).

© The Author(s), 2023. Published by Cambridge University Press on behalf of International Centre for Diffraction Data. This is an Open Access article, distributed under the terms of the Creative Commons Attribution licence (<http://creativecommons.org/licenses/by/4.0/>), which permits unrestricted re-use, distribution and reproduction, provided the original article is properly cited. [doi:10.1017/S0885715622000513]

Key words: toceranib, powder diffraction, Rietveld refinement, density functional theory

I. INTRODUCTION

Toceranib (as its phosphate salt under the brand name Palladia) is a receptor tyrosine kinase inhibitor and is used in the treatment of canine mast cell tumors (London *et al.*, 2009). Toceranib functions by killing tumor cells and decreasing the blood supply to the tumor. The systematic name of the free base (CAS Registry Number 356068-94-5) is 5-[(Z)-(5-fluoro-2-oxo-1H-indol-3-ylidene)methyl]-2,4-dimethyl-N-(2-pyrrolidin-1-ylethyl)-1H-pyrrole-3-carboxamide. A two-dimensional molecular diagram is shown in Figure 1.

The only powder diffraction data of which we are aware was measured in the context of a study of toceranib/nanohydroxyapatite as a drug delivery platform (Sobierajska *et al.*, 2022).

This work was carried out as part of a project (Kaduk *et al.*, 2014) to determine the crystal structures of large-volume commercial pharmaceuticals, and include high-quality powder diffraction data for them in the Powder Diffraction File (Gates-Rector and Blanton, 2019).

II. EXPERIMENTAL AND STRUCTURE REFINEMENT

The toceranib sample was a commercial reagent, purchased from Sigma (Lot #139046), and was used as-received. The certificate of analysis indicated that this was the free base rather than the phosphate salt. The yellow powder was packed into a 1.5 mm diameter Kapton capillary and rotated during the measurement at ~50 Hz. The powder pattern was measured at 295 K at beamline 11-BM (Antao *et al.*, 2008; Lee

et al., 2008; Wang *et al.*, 2008) of the Advanced Photon Source at Argonne National Laboratory using a wavelength of 0.458963(2) Å from 0.5 to 50° 2θ with a step size of 0.001° and a counting time of 0.1 s step⁻¹. The high-resolution powder diffraction data were collected using twelve silicon crystal analyzers that allow for high angular resolution, high precision, and accurate peak positions. A mixture of silicon (NIST SRM 640c) and alumina (NIST SRM 676a) standards (ratio Al₂O₃:Si = 2:1 by weight) was used to calibrate the instrument and refine the monochromatic wavelength used in the experiment.

The pattern was difficult to index, perhaps indicating that the sample was a mixture of phases. We tried progressively permitting a greater number of unindexed lines and using several different indexing programs. Eventually JADE Pro (MDI, 2022) yielded the cell with $a = 10.69345$, $b = 24.52105$, $c = 7.87506$ Å, $\beta = 107.79^\circ$, $V = 1966.27$ Å³, and $Z = 4$. The lowest-angle peak observed in the diffraction pattern (among others) was not indexed by this cell. A reduced cell search in the Cambridge Structural Database (Groom *et al.*, 2016) yielded 20 hits, but no structures of toceranib derivatives. The suggested space group was $P2_1/c$, which was confirmed by successful solution and refinement of the structure. Efforts to identify the unindexed lines with a possible second phase were unsuccessful.

A toceranib molecule was downloaded from PubChem (Kim *et al.*, 2019) as Conformer3D_CID_5319106.sdf. It was converted to a .mol2 file using Mercury (Macrae *et al.*, 2020), and to a Fenske-Hall Z-matrix file using OpenBabel (O'Boyle *et al.*, 2011). The structure was solved by parallel tempering techniques as implemented in FOX (Favre-Nicolin and Černý, 2002), with $(\sin\theta/\lambda)_{\max} = 0.3$ $2\theta_{\max} = 15.8^\circ$. The success rate represented by the FOX cost factor

^{a)} Author to whom correspondence should be addressed. Electronic mail: kaduk@polycrystallography.com

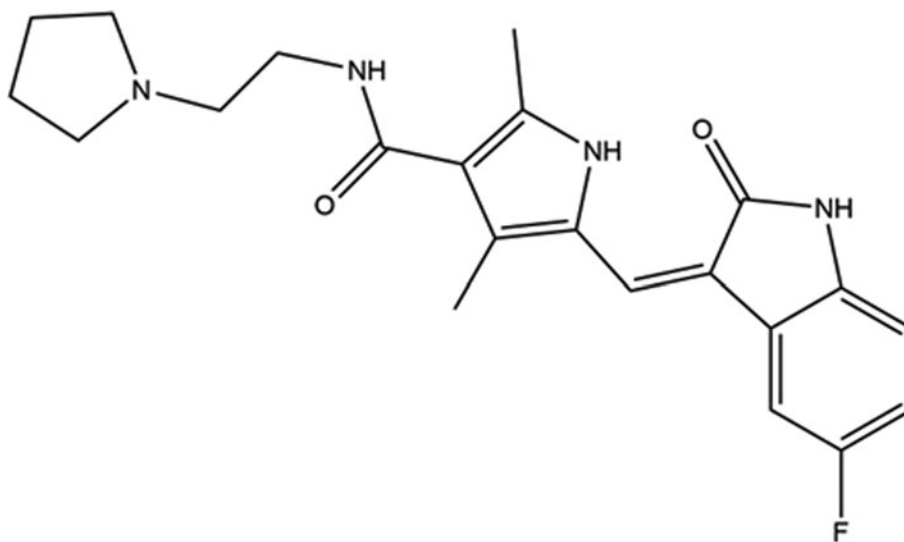


Figure 1. The 2D molecular structure of toceranib.

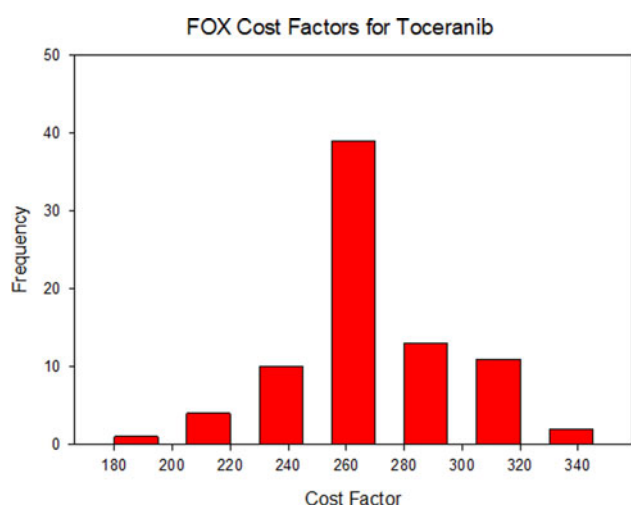


Figure 2. Cost factors (lower is better) for the 81 structure solution runs using FOX. The best solution (used for refinement) is the one with the lowest cost factor.

was low (Figure 2). The best solution (the one with the lowest cost factor) was notable because it contained hydrogen bonds and no voids were apparent. The solutions which were found most often either did not exhibit the expected hydrogen bonds and/or contained voids.

Rietveld refinement was carried out using GSAS-II (Toby and Von Dreele, 2013). Only the 2.0–25.0° portion of the pattern was included in the refinement ($d_{\min} = 1.060 \text{ \AA}$). The unindexed peaks were considered to be due to an impurity and ignored; no excluded regions were used. All non-H bond distances and angles (plus the plane of the fused ring system) were subjected to restraints, based on a Mercury/Mogul Geometry Check (Bruno *et al.*, 2004; Sykes *et al.*, 2011). The Mogul average and standard deviation for each quantity were used as the restraint parameters. The restraints contributed 9.1% to the final χ^2 . The hydrogen atoms were included in calculated positions, which were recalculated during the refinement using Materials Studio (Dassault, 2021). The U_{iso} of the heavy atoms were grouped by chemical

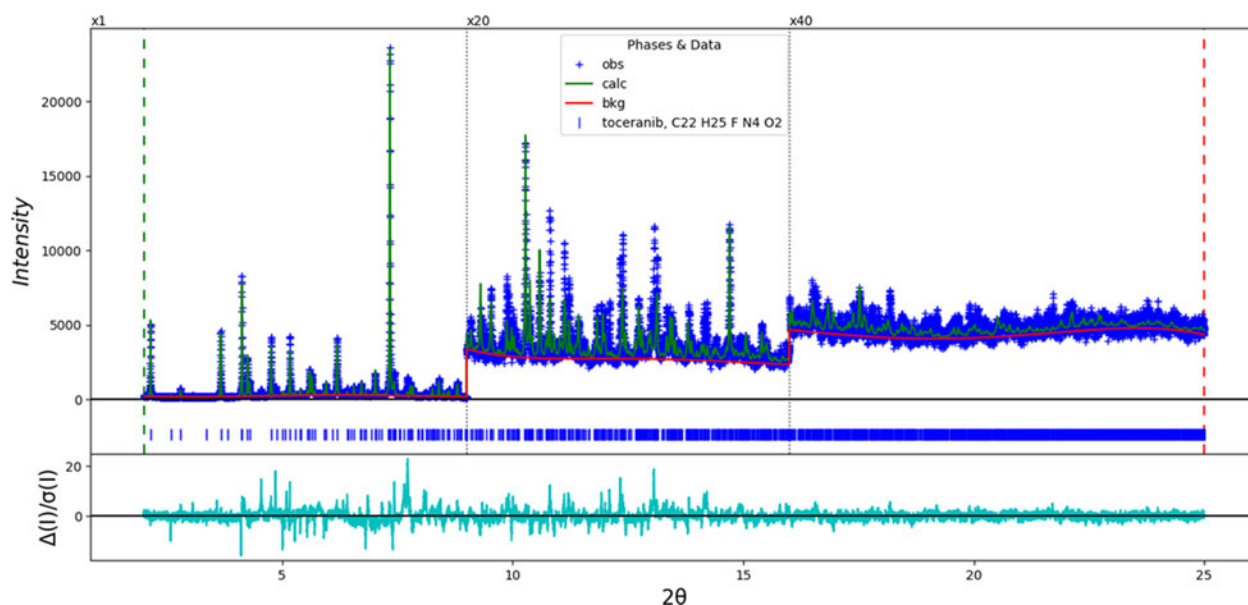


Figure 3. The Rietveld plot for the refinement of toceranib. The blue crosses represent the observed data points, and the green line is the calculated pattern. The cyan curve is the normalized error plot. The vertical scale has been multiplied by a factor of 10 \times for $2\theta > 9.0^\circ$ and by a factor of 40 \times for $2\theta > 16.0^\circ$. The row of blue tick marks indicates the calculated reflection positions for toceranib.

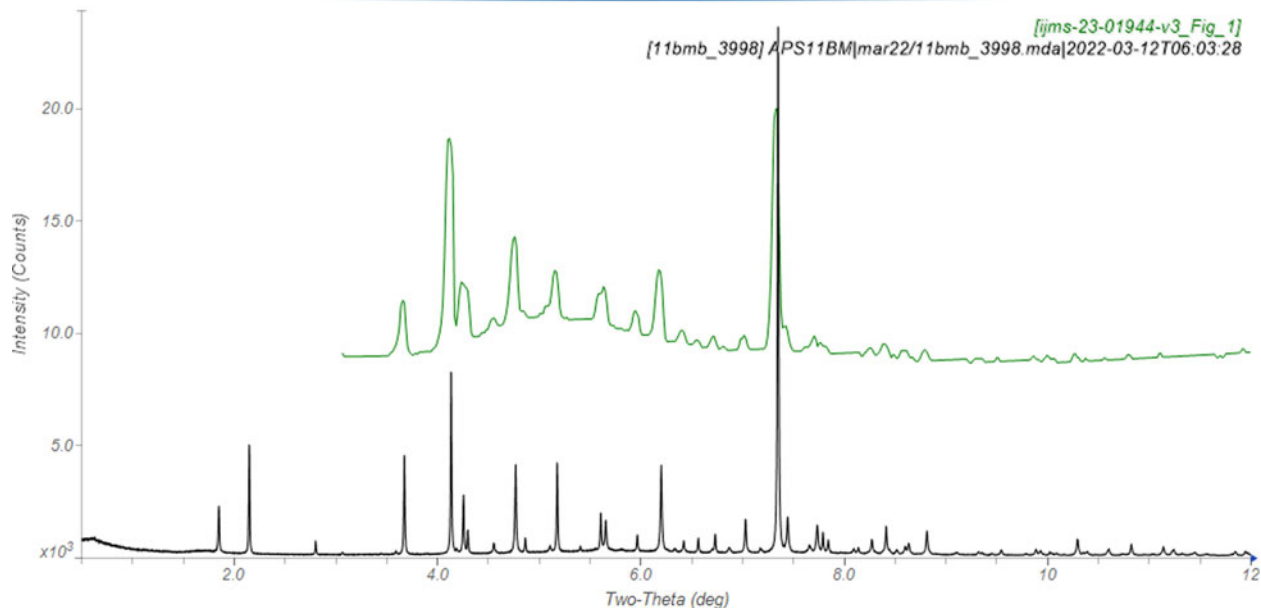


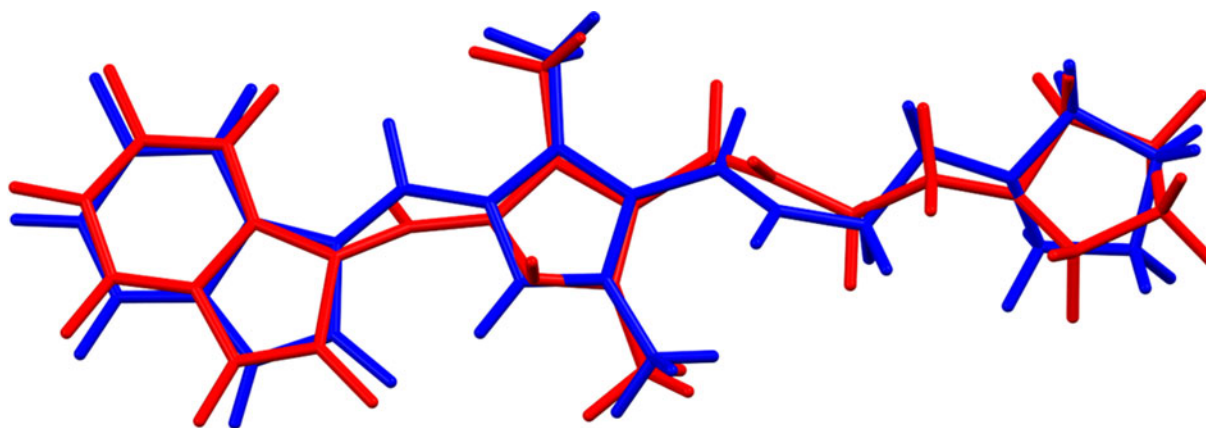
Figure 4. Comparison of the synchrotron pattern of toceranib (black) to that reported by Sobierajska *et al.* (2022; green). The literature pattern, measured using $\text{CuK}\alpha$ radiation, was digitized using UN-SCAN-IT (Silk Scientific, 2013) and was converted to the synchrotron wavelength of 0.458963 Å using JADE Pro (MDI, 2022). Image generated using JADE Pro (MDI, 2022).

similarity. The U_{iso} for the H atoms were fixed at $1.3 \times$ the U_{iso} of the heavy atoms to which they are attached. A second-order spherical harmonic preferred orientation model was included in the refinement. The refined texture index was 1.019(1). The peak profiles were described using the generalized micro-strain model. The background was modeled using a 6-term shifted Chebyshev polynomial, and a peak at $6.00^\circ 2\theta$ to model the scattering from the Kapton capillary and any amorphous component.

The final refinement (started from the result of the DFT calculation) of 113 variables using 23 037 observations and 79 restraints yielded the residuals $R_{\text{wp}} = 0.1586$ and $\text{GOF} = 2.49$. The largest peak (0.46 Å from C21) and hole (0.96 Å

from N7) in the difference Fourier map were 0.67(16) and $-0.63(16) e\text{Å}^{-3}$, respectively. The largest positive errors in the difference plot (Figure 3) are at the unindexed impurity peaks, and some negative errors occur at toceranib peaks.

The crystal structure was optimized using VASP (Kresse and Furthmüller, 1996) (fixed experimental unit cell) through the MedeA graphical interface (Materials Design, 2016). The calculation was carried out on 16 2.4 GHz processors (each with 4 GB RAM) of a 64-processor HP Proliant DL580 Generation 7 Linux cluster at North Central College. The calculation used the GGA-PBE functional, a plane wave cutoff energy of 400.0 eV, and a k -point spacing of 0.5Å^{-1} leading to a $2 \times 1 \times 2$ mesh, and took ~ 101.1 h. A single-point density



Rmsd = 0.550

Figure 5. Comparison of the Rietveld-refined (red) and VASP-optimized (blue) structures of toceranib. The rms Cartesian displacement is 0.550 Å. Image generated using Mercury (Macrae *et al.*, 2020).

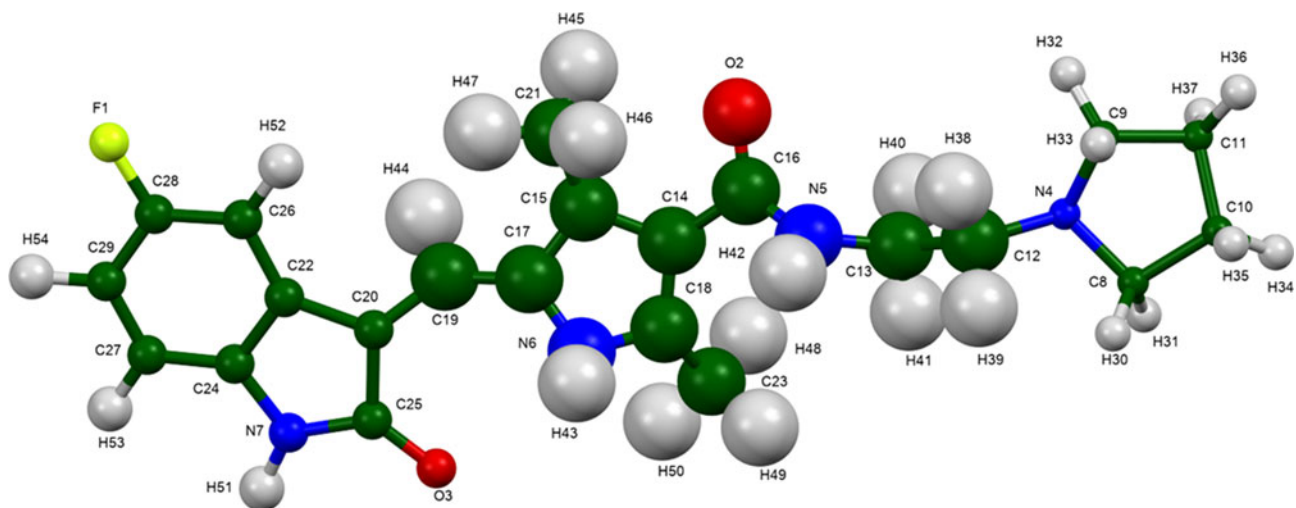


Figure 6. The asymmetric unit of toceranib, with the atom numbering. The atoms are represented by 50% probability spheroids. Image generated using Mercury (Macrae *et al.*, 2020).

functional calculation (fixed experimental cell) and population analysis were carried out using CRYSTAL17 (Dovesi *et al.*, 2018). The basis sets for the H, C, N, and O atoms in the calculation were those of Gatti *et al.* (1994), and that for F was that of Peintinger *et al.* (2013). The calculations were run on a 3.5 GHz PC using 8 *k*-points and the B3LYP functional, and took ~8.3 h.

III. RESULTS AND DISCUSSION

The synchrotron powder pattern of this study matches the pattern measured by Sobierajska *et al.* (2022) well enough to conclude that they represent the same material (Figure 4). The

limited range and quality of the literature pattern makes the comparison difficult, but it seems that our sample is representative. The root-mean-square (rms) Cartesian displacement between the Rietveld-refined and DFT-optimized structures of toceranib is 0.550 Å (Figure 5). This agreement is outside of the normal range for correct structures (van de Streek and Neumann, 2014). We suspect that the Rietveld refinement has distorted the structure to account for some of the intensity of the unindexed impurity peaks. This discussion concentrates on the DFT-optimized structure. The asymmetric unit (with atom numbering) is illustrated in Figure 6. The U_{iso} of the atoms in the central portion of the molecule are larger than those on the ends. The best view of the crystal structure is

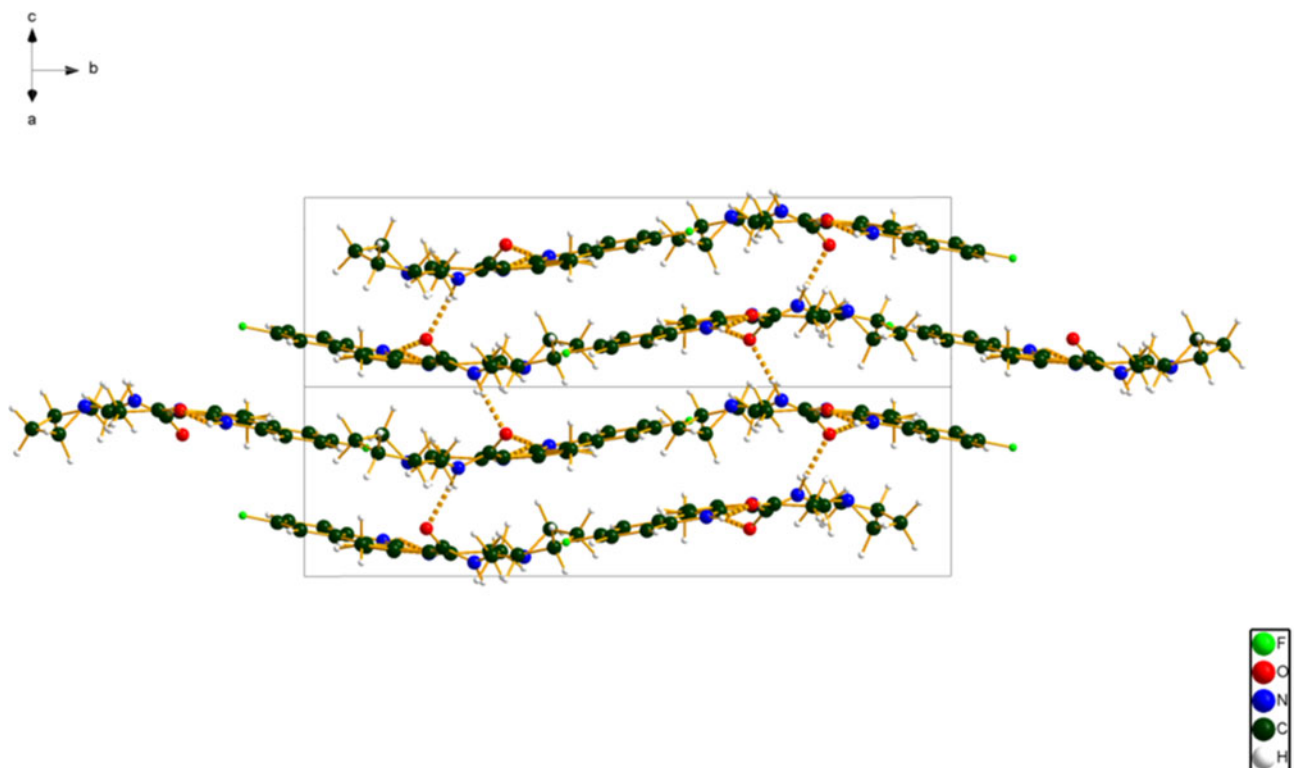


Figure 7. The crystal structure of toceranib, viewed down the [101] direction. Image generated using Diamond (Crystal Impact, 2022).

TABLE I. Unusual torsion angles (Mercury/Mogul geometry analysis) in toceranib.

Torsion angle	Value (°)	Description
C13–C12–N4–C8	49.8	Tail of gauche portion of gauche/trans distribution
O2–C16–N5–C13	–24.1	Tail of a planar distribution
C14–C16–N5–C13	152.3	Tail of trans distribution
N5–C13–C12–N4	158.0	Tail of trans portion of mainly gauche distribution

down the [101] direction (Figure 7). The crystal structure consists of stacks of approximately planar molecules, with hydrogen bonds between the layers. The approximate plane of the fused ring system is (-5-46).

Almost all of the bond distances and bond angles fall within the normal ranges indicated by a Mercury/Mogul Geometry check (Macrae *et al.*, 2020). The C12–C13–N5 angle of 118.2° (average = 111.6(19)°, Z-score = 3.4) is flagged as unusual. Four torsion angles are flagged as unusual (Table I). These describe the conformation of the chain linking the pyrrolidine ring to the rest of the molecule.

The quantum chemical geometry optimization of the toceranib molecule (DFT/B3LYP/6-31G*/water) using Spartan '18 (Wavefunction, 2020) indicated that the observed conformation is 10.2 kcal mol⁻¹ higher in energy than the local minimum, which has a different orientation of the pyrrolidine ring. A conformational analysis (MMFF force field) indicates that the minimum-energy conformation is 1.8 kcal mol⁻¹ lower in energy, but has conformational differences throughout the molecule. The molecule is apparently flexible, and intermolecular interactions are important in determining the solid-state conformation.

TABLE II. Hydrogen bonds (CRYSTAL17) in toceranib.

H-Bond	D-H (Å)	H...A (Å)	D...A (Å)	D-H...A (°)	Overlap (ϵ)	E (kcal mol ⁻¹)
N6–H43...O3	1.054	1.627 ^a	2.628	156.8	0.085	6.7
N5–H42...O2	1.029	1.830	2.794	154.5	0.056	5.5
N7–H51...O2	1.027	2.101	3.118	170.0	0.041	4.7
C13–H40...C14	1.102	2.658	3.714	160.2	0.010	
H33...H39		2.335 ^a			0.013	

^aIntramolecular.

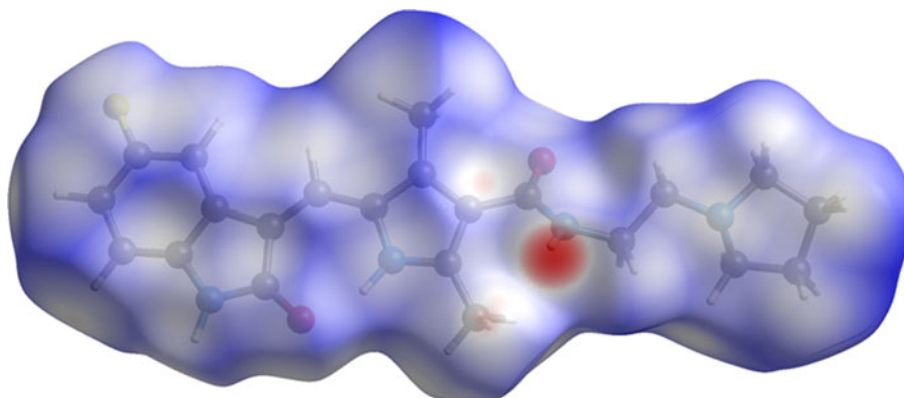


Figure 8. The Hirshfeld surface of toceranib. Intermolecular contacts longer than the sums of the van der Waals radii are colored blue, and contacts shorter than the sums of the radii are colored red. Contacts equal to the sums of radii are white. Image generated using CrystalExplorer (Turner *et al.*, 2017).

Analysis of the contributions to the total crystal energy of the structure using the Forcite module of Materials Studio (Dassault, 2021) suggests that the intramolecular deformation energy is dominated by angle distortion terms. The intermolecular energy is dominated by electrostatic attractions, which in this force field analysis include hydrogen bonds. The hydrogen bonds are better analyzed using the results of the DFT calculation.

The most prominent hydrogen bonds are N–H...O (Table II). The intramolecular N5–H42...O3 hydrogen bond is very strong. The energies of the N–H...O hydrogen bonds were calculated using the correlation of Wheatley and Kaduk (2019). The N5–H42...O2 and N7–H51...O2 hydrogen bonds link the layers. There is one C–H...C hydrogen bond, as well as an intramolecular 1,3 H...H interaction.

The volume enclosed by the Hirshfeld surface of toceranib (Figure 8; Hirshfeld, 1977; Turner *et al.*, 2017) is 482.70 Å³, 98.26% of 1/4 the unit cell volume. The packing density is thus fairly typical. The only significant close contacts (red in Figure 8) involve the hydrogen bonds. The volume/non-hydrogen atom is typical at 16.9 Å³.

The Bravais–Friedel–Donnay–Harker (Bravais, 1866; Friedel, 1907; Donnay and Harker, 1937) morphology suggests that we might expect blocky morphology for toceranib, with {010} as principal faces. A second-order spherical harmonic preferred orientation model was included in the refinement. The texture index was 1.019(1), indicating that preferred orientation was not significant for this rotated capillary specimen.

IV. DEPOSITED DATA

The powder pattern of toceranib from this synchrotron data set has been submitted to ICDD for inclusion in the

Powder Diffraction File. The Crystallographic Information Framework (CIF) files containing the results of the Rietveld refinement (including the raw data) and the DFT geometry optimization were deposited with the ICDD. The data can be requested at pdj@icdd.com.

ACKNOWLEDGEMENTS

The use of the Advanced Photon Source at Argonne National Laboratory was supported by the U.S. Department of Energy, Office of Science, Office of Basic Energy Sciences, under Contract No. DE-AC02-06CH11357. This work was partially supported by the International Centre for Diffraction Data. We thank Lynn Ribaud and Saul Lapidus for their assistance in the data collection.

CONFLICT OF INTEREST

The authors have no conflict of interest to declare.

REFERENCES

- Antao, Sytle M., Ishmael Hassan, Jun Wang, Peter L. Lee, and Brian H. Toby. 2008. "State-of-the-Art High-Resolution Powder X-Ray Diffraction (HRPXRD) Illustrated with Rietveld Structure Refinement of Quartz, Sodalite, Tremolite, and Meionite." *The Canadian Mineralogist* 46 (6): 1501–9.
- Bravais, Auguste. 1866. *Etudes Cristallographiques*. Paris, Gauthier-Villars.
- Bruno, Ian J., Jason C. Cole, Magnus Kessler, Jie Luo, WD Sam Motherwell, Lucy H. Purkis, Barry R. Smith, Robin Taylor, Richard I. Cooper, Stephanie E. Harris, and A. Guy Orpen. 2004. "Retrieval of Crystallographically-Derived Molecular Geometry Information." *Journal of Chemical Information and Computer Sciences* 44 (6): 2133–44.
- Dassault Systèmes. 2021. *Materials Studio 2021*. San Diego, CA, BIOVIA.
- Donnay, J. D H., and David Harker. 1937. "A New Law of Crystal Morphology Extending the Law of Bravais." *American Mineralogist: Journal of Earth and Planetary Materials* 22 (5): 446–67.
- Dovesi, Roberto, Alessandro Erba, Roberto Orlando, Claudio M. Zicovich-Wilson, Bartolomeo Civalieri, Lorenzo Maschio, Michel Rérat, Silvia Casassa, Jacopo Baima, Simone Salustro, and Bernard Kirtman. 2018. "Quantum-Mechanical Condensed Matter Simulations with CRYSTAL." *Wiley Interdisciplinary Reviews: Computational Molecular Science* 8 (4): e1360.
- Favre-Nicolin, Vincent, and Radovan Černý. 2002. "FOX, 'Free Objects for Crystallography': A Modular Approach to Ab Initio Structure Determination from Powder Diffraction." *Journal of Applied Crystallography* 35 (6): 734–43.
- Friedel, Georges. 1907. "Etudes sur la loi de Bravais." *Bulletin de Minéralogie* 30 (9): 326–455.
- Gates-Rector, Stacy, and Thomas Blanton. 2019. "The Powder Diffraction File: A Quality Materials Characterization Database." *Powder Diffraction* 34 (4): 352–60.
- Gatti, C., V. R. Saunders, and C. Roetti. 1994. "Crystal Field Effects on the Topological Properties of the Electron Density in Molecular Crystals: The Case of Urea." *The Journal of Chemical Physics* 101 (12): 10686–96.
- Groom, C. R., Bruno, I. J., Lightfoot, M. P., and Ward, S. C. 2016. "The Cambridge Structural Database." *Acta Crystallographica Section B. Structural Science, Crystal Engineering and Materials* 72, 171–9.
- Hirshfeld, Fred L. 1977. "Bonded-Atom Fragments for Describing Molecular Charge Densities." *Theoretica Chimica Acta* 44 (2): 129–38.
- Kaduk, James A., Cyrus E. Crowder, Kai Zhong, Timothy G. Fawcett, and Matthew R. Suchomel. 2014. "Crystal Structure of Atomoxetine Hydrochloride (Strattera), C17H22NOCl." *Powder Diffraction* 29 (3): 269–73.
- Kim, Sunghwan, Jie Chen, Tiejun Cheng, Asta Gindulyte, Jia He, Siqian He, Qingliang Li, Benjamin A. Shoemaker, Paul A. Thiessen, Bo Yu, Leonid Zaslavsky, Jian Zhang, and Evan E. Bolton. 2019. "PubChem 2019 Update: Improved Access to Chemical Data." *Nucleic Acids Research* 47 (D1): D1102–9. doi:10.1093/nar/gky1033.
- Kresse, Georg, and Jürgen Furthmüller. 1996. "Efficiency of Ab-Initio Total Energy Calculations for Metals and Semiconductors Using a Plane-Wave Basis Set." *Computational Materials Science* 6 (1): 15–50.
- Lee, Peter L., Deming Shu, Mohan Ramanathan, Curt Preissner, Jun Wang, Mark A. Beno, Robert B. Von Dreele, Lynn Ribaud, Charles Kurtz, Sytle M. Antao, Xuesong Jiao, and Brian H. Toby. 2008. "A Twelve-Analyzer Detector System for High-Resolution Powder Diffraction." *Journal of Synchrotron Radiation* 15 (5): 427–32.
- London, Cheryl A., Phyllis B. Malpas, Stacey L. Wood-Follis, Joseph F. Boucher, Anthony W. Rusk, Mona P. Rosenberg, Carolyn J. Henry, Kathy L. Mitchener, Mary K. Klein, John G. Hintermeister, Philip J. Bergman, Guillermo C. Couto, Guy N. Mauldin, Gina M. Michels. 2009. "Multi-Center, Placebo-Controlled, Double-Blind, Randomized Study of Oral Toceranib Phosphate (SU11654), a Receptor Tyrosine Kinase Inhibitor, for the Treatment of Dogs with Recurrent (Either Local or Distant) Mast Cell Tumor Following Surgical Excision." *Clinical Cancer Research* 15 (11): 3856–65.
- Macrae, Clare F., Ioana Sovago, Simon J. Cottrell, Peter T. A. Galek, Patrick McCabe, Elna Pidcock, Michael Platings, Greg P. Shields, Joanna S. Stevens, Matthew Towler, and Peter A. Wood. 2020. "Mercury 4.0: From Visualization to Analysis, Design and Prediction." *Journal of Applied Crystallography* 53 (1): 226–35.
- Materials Design. 2016. *Medea 2.20.4*. Angel Fire, NM, Materials Design Inc.
- MDI. 2022. "JADE Pro version 8.2." Livermore, CA, USA, MDI Materials Data.
- O'Boyle, Noel M., Michael Banck, Craig A. James, Chris Morley, Tim Vandermeersch, and Geoffrey R. Hutchison. 2011. "Open Babel: An Open Chemical Toolbox." *Journal of Cheminformatics* 3 (1): 1–14.
- Peintinger, Michael F., Daniel Vilela Oliveira, and Thomas Bredow. 2013. "Consistent Gaussian Basis Sets of Triple-Zeta Valence with Polarization Quality for Solid-State Calculations." *Journal of Computational Chemistry* 34 (6): 451–9.
- Putz, Crystal Impact-Dr H., and Dr K. Brandenburg. 2022. "Diamond-Crystal and Molecular Structure Visualization. Kreuzherrenstr. 102, 53227 Bonn, Germany." <https://www.crystalimpact.de/diamond>.
- Silk Scientific. 2013. *UN-SCAN-IT 7.0*. Silk Scientific, Orem, UT.
- Sobierajska, Paulina, Anna Serwotka-Suszczak, Sara Targonska, Damian Szymanski, Krzysztof Marycz, and Rafal J. Wiglusz. 2022. "Synergistic Effect of Toceranib and Nanohydroxyapatite as a Drug Delivery Platform—Physicochemical Properties and In Vitro Studies on Mastocytoma Cells." *International Journal of Molecular Sciences* 23 (4): 1944. doi: 10.3390/ijms23041944
- Sykes, Richard A., Patrick McCabe, Frank H. Allen, Gary M. Battle, Ian J. Bruno, and Peter A. Wood. 2011. "New Software for Statistical Analysis of Cambridge Structural Database Data." *Journal of Applied Crystallography* 44 (4): 882–6.
- Toby, Brian H., and Robert B. Von Dreele. 2013. "GSAS-II: The Genesis of a Modern Open-Source All Purpose Crystallography Software Package." *Journal of Applied Crystallography* 46 (2): 544–9.
- Turner, M. J., J. J. McKinnon, S. K. Wolff, D. J. Grimwood, P. R. Spackman, D. Jayatilaka, and M. A. Spackman. 2017. *CrystalExplorer17*: 76730. <http://hirshfeldsurface.net>.
- van de Streek, Jacco, and Marcus A. Neumann. 2014. "Validation of Molecular Crystal Structures from Powder Diffraction Data with Dispersion-Corrected Density Functional Theory (DFT-D)." *Acta Crystallographica. Section B, Structural Science, Crystal Engineering and Materials* 70 (Pt 6): 1020–32.
- Wang, Jun, Brian H. Toby, Peter L. Lee, Lynn Ribaud, Sytle M. Antao, Charles Kurtz, Mohan Ramanathan, Robert B. Von Dreele, and Mark A. Beno. 2008. "A Dedicated Powder Diffraction Beamline at the Advanced Photon Source: Commissioning and Early Operational Results." *Review of Scientific Instruments* 79 (8): 085105.
- Wavefunction, Inc. 2020. "Spartan '18" Version 1.4.5. Irvine, CA, Wavefunction, Inc.
- Wheatley, Austin M., and James A. Kaduk. 2019. "Crystal Structures of Ammonium Citrates." *Powder Diffraction* 34 (1): 35–43.